



In-situ incorporation of iron-copper bimetallic particles in electrospun carbon nanofibers as an efficient Fenton catalyst

Jing Wang, Chao Liu, Jiansheng Li*, Rui Luo, Xingru Hu, Xiuyun Sun, Jinyou Shen, Weiqing Han, Lianjun Wang*

Jiangsu Key Laboratory of Chemical Pollution Control and Resources Reuse, School of Environmental and Biological Engineering, Nanjing University of Science and Technology, Nanjing 210094, PR China

ARTICLE INFO

Article history:

Received 30 November 2016
Received in revised form 27 January 2017
Accepted 9 February 2017
Available online 12 February 2017

Keywords:

Carbon nanofibers
Heterogeneous Fenton
Iron-copper bimetallic
Acid Orange II
Nanofibrous structure

ABSTRACT

Iron-copper bimetallic nanoparticles supported on carbon nanofibers as a composite catalyst (FeCu/CNF) was prepared for the first time in this work. The iron-copper bimetallic nanoparticles were formed in situ by carbothermic reduction during the carbonization process. The characterization results show that the FeCu/CNF possesses fibrous morphology, porous structure with high specific surface area, and dispersed iron-copper nanoparticles. For comparison, three other catalysts, including solely iron nanoparticles supported on carbon nanofibers (Fe/CNF), solely copper nanoparticles supported on carbon nanofibers (Cu/CNF) and iron-copper nanoparticles supported on blocky carbon matrixes (FeCu/C) were also prepared. The heterogeneous Fenton catalytic performance of synthesized catalyst was evaluated by degrading a typical azo dye, Acid Orange II (AOII). The results show that almost 97.7% of 100 mg/L AOII is removed by FeCu/CNF in reaction time of 1 h, which is much higher than those of comparison catalysts operated in the same experimental condition. Additionally, the FeCu/CNF also reveals a wider pH adaptation ability compared with Fe/CNF. Based on the results of •OH detection and resistance of mass transfer testing in catalysts, the remarkable catalytic performance of FeCu/CNF is considered as the synergistic effect of iron and copper and the superiority of nanofibrous structure in catalyst. The good stability and recoverability of FeCu/CNF were also demonstrated. The as-synthesized catalyst is proved to be an attractive candidate in heterogeneous Fenton chemistry.

© 2017 Elsevier B.V. All rights reserved.

1. Introduction

Nowadays, the scarcity of water resources and the increasing of water contamination have been a worldwide environmental problem, and have drawn extensive attention from both the public and researchers [1–3]. Among the water pollutants, azo dyes constitute a particular group of nitrogen-to-nitrogen double bond (N=N), are the most pervasive synthetic dyes used in industry, which have brought serious eco-environmental problems due to their toxicity, recalcitrance, non-biodegradability and carcinogenicity [4–6]. The conventional methods used in wastewater treatment such as biological process and physical adsorption are limited because the azo dyes are difficult to be completely degraded by these methods [5–8]. Recently, advanced oxidation technologies (AOTs) have been demonstrated as a highly efficient process for destructing and

degrading organic pollutants [9]. As an alternative to AOTs, Fenton technology, which can generate hydroxyl radicals (•OH) through the catalytic reaction of iron in the present of H₂O₂, has been of great interest and widely used owing to its environment-friendly and easy operation [10,11]. Homogeneous Fenton catalysts, such as Fe²⁺/Fe³⁺, have been proven to be highly active. However, there still are some disadvantages, such as narrow pH operating conditions, unrecyclability and large amount of iron-containing sludge in effluent [12–14]. To resolve these problems, heterogeneous Fenton catalysts have been developed by using solid catalysts such as zero-valent iron and iron oxide minerals to replace iron salts [15–18]. However, whether for the homogeneous or heterogeneous Fenton process, the iron based catalysts show relative inert activity when conducted at high pH values. To improve the catalytic efficiency of the catalysts, other power supplies are always needed, which will increase the treatment cost [19,20].

In the recent years, another metal species, copper, which possesses a similar role as iron based heterogeneous Fenton catalyst, has triggered considerable research interest due to its wide pH range adapting property. Moreover, because of the positive syn-

* Corresponding authors.

E-mail addresses: lijsh@mail.njust.edu.cn (J. Li), [\(L. Wang\)](mailto:wanglj@mail.njust.edu.cn).

ergistic effects between iron and copper, which could enhance the catalytic performance of catalyst, integrating of copper with iron to construct iron-copper bimetallic nanoparticles as the heterogeneous catalyst has become a hotspot in Fenton chemistry [8,14,19]. Nevertheless, nanoparticles always tend to be aggregated due to its inherent high surface energy [20], which inevitably impose detrimental effects to the catalytic activity and stability of catalyst [21]. To improve the catalytic activity and stability of the nanoparticles, the supporting strategy, which incorporates iron-copper bimetallic nanoparticles with various supports, such as zeolite [22], clay [23], MCM-41 [24], mesoporous carbon [25–27], SBA-15 [28] and ZSM-5 [29], has been widely explored. By using these novel supports, remarkable improvements were achieved. However, the structure of supports are normally based on a two dimensionally confined space, which may limit the electron transport and reactant diffusion, and thus limit the efficiency of catalysis reaction [30].

Recently, one dimensional (1D) nanostructures have received a great attention due to their electrical, optical, sensing and catalytic property [31]. With the rapid development of electro-spinning technique, it provides a facile and cost-effective way to produce 1D nanofibers [32,33]. As previous reports [34,35], 1D nanofibrous structures have showed a superior catalytic activity in many reactions because of their high axial ratio aspect, which allow a fast and long-distance electron transport. Among them, porous carbon nanofibers, which are able to promote the kinetics of electron transfer reaction and enhance the catalytic activity, have a special interest in the field of catalyst [35]. Moreover, the porous structure of the supports also can enhance the dispersibility and stability of the metallic nanoparticles and the accessibility of the active sites [36–38]. Liu et al. has fabricated Pd_xCo_y nanoparticle/carbon nanofiber composites as an electrocatalyst, which showed enhanced electrocatalytic activity and stability in formic acid and methanol oxidation reactions [39]. Xie et al. has prepared $\text{ZnFe}_2\text{O}_4/\text{Fe}_3\text{O}_4/\text{Ag}$ nanoparticle-loaded mesoporous carbon fibers as a photocatalyst and displayed high photocatalytic activity toward the degradation of methylene blue and methyl orange under visible light irradiation [40]. Actually, various metallic nanoparticles have been supported on carbon nanofibers as the composite catalysts and have exhibited high catalytic activity. However, the application of this distinctive 1D catalyst in heterogeneous Fenton catalysis has been rarely reported. As mentioned above, iron-copper bimetallic nanoparticle is a highly efficient Fenton catalyst. Actually, up to now, the advantage of carbon nanofibers decorated by iron-copper bimetallic as composite catalyst has not been exploited. Therefore, it is highly desired to explore the facile preparation of carbon nanofibers decorated by iron-copper bimetallic nanoparticles and the heterogeneous Fenton catalytic property of this new composite catalyst.

In this work, the iron-copper bimetallic nanoparticles supported on carbon nanofibers as a composite catalyst (FeCu/CNF) were prepared by electrospinning technique and followed by the carbonization of electrospun nanofibers, which contains polyacrylonitrile, iron (III) acetylacetone and copper (II) acetate monohydrate. The iron-copper bimetallic nanoparticles were formed in situ by carbothermic reduction during the carbonization process. The heterogeneous Fenton catalytic performance of synthesized catalyst was evaluated by degradation of a typical azo dye, Acid Orange II. For comparison, three other catalysts, including solely iron nanoparticles supported on carbon nanofibers (Fe/CNF), solely copper nanoparticles supported on carbon nanofibers (Cu/CNF) and iron-copper nanoparticles supported on blocky carbon matrixes (FeCu/C) were also prepared. Furthermore, the possible mechanism was proposed by detecting the generation of $\cdot\text{OH}$ and testing the resistance of mass transfer in

these catalysts. Finally, the stability and reusability of the catalyst was investigated.

2. Experimental

2.1. Chemicals

Analytical reagents including iron (III) acetylacetone ($\text{Fe}(\text{acac})_3$), copper (II) acetate monohydrate ($\text{Cu}(\text{ac})_2 \cdot \text{H}_2\text{O}$), N,N-dimethylformamide (DMF), hydrogen peroxide (H_2O_2 , 30 wt%), nitric acid (HNO_3 , 65 wt%), sodiumhydroxide (NaOH) and Acid Orange II (AOII) were purchased from Sinopharm Chemical Reagent Co., Ltd. Polyacrylonitrile (PAN, $M_w = 150,000$) was purchased from Sigma-Aldrich. Benzoic acid (BA) and P-hydroxy benzoic acid (p-HBA) were purchased from ANPEL Scientific Instruments (Shanghai) Co., Ltd. 5,5-dimethyl-1-pyrroline N-oxide (DMPO) was purchased from J&K Scientific Ltd. All chemicals were used as received without any further purification. Deionized water (Millipore) was used in all experiments.

2.2. Synthesis of iron-copper bimetallic carbon nanofibers

The typical experimental procedures of iron-copper bimetallic carbon nanofibers are as follows: 3 mmol $\text{Cu}(\text{ac})_2 \cdot \text{H}_2\text{O}$, 1 mmol $\text{Fe}(\text{acac})_3$ and 1 g PAN were added in 20 mL DMF. Then, a homogeneous precursor solution was obtained by magnetic stirring for 2 h at 60 °C. During the electrospinning process, the precursor solution was transported to a syringe pump with a metal needle and the flow rate of spinning solution was 1.47 mL/h. A flat aluminum foil was used as a fiber collector, which was 15 cm away from the metal needle. A positive voltage of 18 kV was applied between the needle and the collector to obtain a stable continuous PAN-based nanofibers (FeCu/PANNF). Before the carbonization, the as obtained electrospun nanofibers were firstly stabilized by heating in air at 240 °C for 3 h with a heating rate of 1 °C/min. Then, the iron-copper bimetallic carbon nanofibers (FeCu/CNF) were obtained after carbonization, which were pyrolyzed in tube furnace at 900 °C for 2 h with a heating rate of 5 °C/min under nitrogen. The Fe/PANNF and Cu/PANNF were fabricated by adding the 4 mmol of corresponding metallic precursor in spinning solution with the similar electrospinning process of FeCu/PANNF . The FeCu/PAN was synthesized by using the same precursor of FeCu/PANNF without electrospinning process. The Fe/CNF , Cu/CNF and FeCu/C were derived from the Fe/PANNF , Cu/PANNF and FeCu/PAN by carbonization, respectively.

2.3. Characterization

X-ray diffraction (XRD) patterns of samples were measured on a Bruker AXS D8 advance powder diffraction system using $\text{Cu K}\alpha$ ($\lambda = 1.5418 \text{ \AA}$). The X-ray photoelectron spectra (XPS) of samples were characterized by PHI Quantera II ESCA System with Al $\text{K}\alpha$ radiation at 1486.8 V. Nitrogen adsorption-desorption isotherms were collected at 77 K by Micromeritics 2020 analyzer (USA). The morphology and structure of samples were examined by scanning electron microscope (SEM) (Quanta 250F operating at 20 kV) and transmission electron microscope (TEM) (TECNAL G2 20 LaB6 operating at 200 kV). STEM-EDS images were performed by JEOL 2100F field emission electron microscope, equipped with Oxford X-Max 80 TLE energy-dispersive spectrometer. The leaching iron and copper ions of samples were determined by atomic absorption spectrometer (AAS) (PinAAcle 900T, PerkinElmer, USA). The electrochemical impedance spectroscopy (EIS) measurements were operated on electrochemical workstation (CHI660E, CH Instrument, Shanghai) in 0.1 M KOH solution with a three-electrode mode, including a work electrode, a platinum wire as the counter

electrode, and Ag/AgCl as the reference electrode. The work electrodes were prepared by well mixing 10 wt% of acetylene black, 80 wt% of sample, and 10 wt% of polytetrafluoroethylene (PTFE), then pressing the obtained mixture onto graphite plate with the 1 cm² reacting area and drying in vacuum oven at 120 °C overnight. Electron spin resonance (ESR) spectroscopy measurements were obtained on a Bruker EMX 10/12 with Microwave Bridge (microwave frequency, x-band; microwave power, 20 mW; modulation amplitude, 1G; modulation frequency, 100KHz) at room temperature.

2.4. Catalytic performance

To explore the catalytic activity of the samples, a series of batch experiments were carried out to degrade 100 mg/L Orange II. Typically, 0.005 g of catalyst was added in a 50 mL flask with 10 mL of Orange II solution. The pH of the reaction medium was adjusted by using an appropriate amount of 0.1 M NaOH or 0.1 M HNO₃ to a given value. Then, a certain amount of H₂O₂ (30 wt%) was added to the suspension and initiated the degradation reaction. All of the covered flasks were kept at a 30 °C in a thermostatic air bath oscillator with a constant speed of 200 rpm. Each flask was taken out from the bath at different time intervals, and the supernatant solution was collected by filtration for UV-vis absorbance analysis (a universal microplate spectrophotometer PowerWave XS) and total organic carbon (TOC) analyzer (Vario TOC Cube, Elementar Analysensysteme GrmbH). The quantitation of hydroxyl radicals were determined by a previous reported method in literatures [14,41]. The used catalysts were regenerated by centrifugation then washing with methanol for stability tests.

3. Results and discussion

3.1. Physicochemical and morphology properties of catalysts

To investigate the crystal structure of metals in obtained carbonic samples, the wide-angle XRD pattern of these samples are performed. As shown in Fig. 1, a diffraction peak centered at 2θ of 44.6° is detected in Fe/CNF, which can be referred to the (110) diffraction of α-Fe (JCPDS No. 06-0696). In the sample of Cu/CNF, four well-resolved diffraction peaks at 2θ values of 43.2, 50.4, 74.1 and 89.9°, which can be indexed to (111), (200), (220) and (311) diffractions of Cu (JCPDS No. 99-0034), respectively. Both the (110) diffraction of α-Fe and (111) diffraction of Cu can be observed in FeCu/CNF and FeCu/C simultaneously, indicating the successful loading of iron and copper in these two samples. The iron and copper elements are further analyzed by XPS, and the obtained results are shown in Fig. 2. For the Fe 2p spectrum (Fig. 2A), the photoelectron peaks at binding energies of 707 eV correspond to the Fe 2p_{3/2} of zero-valent iron (ZVI) [42], which are observed in Fe/CNF, FeCu/CNF and FeCu/C. Moreover, three other peaks in these samples at binding energies of 711, 720 and 725 eV are also found, which are assigned to Fe 2p_{3/2}, shake-up satellite of Fe 2p_{3/2} and Fe 2p_{1/2} of Fe³⁺, respectively [43]. The emerging photoelectron peaks of Fe³⁺ may attribute to the easy oxidation of ZVI in air, which could result in a layer of iron oxide around the ZVI nanoparticles [44,45]. The Cu 2p spectrum of samples are shown in Fig. 2B. Two photoelectron peaks at binding energies of 932 and 952 eV can be observed in Cu/CNF, FeCu/CNF and FeCu/C, which are assigned to Cu 2p_{3/2} and Cu 2p_{1/2} of zero-valent copper, respectively [46]. The results from XRD and XPS demonstrate that the expected active component of catalysts have been achieved.

The corresponding superficial morphology of obtained samples are characterized by SEM. As shown in Fig. S1, FeCu/PAN (Fig. S1D) possesses bulky and ruleless morphology, which was pre-

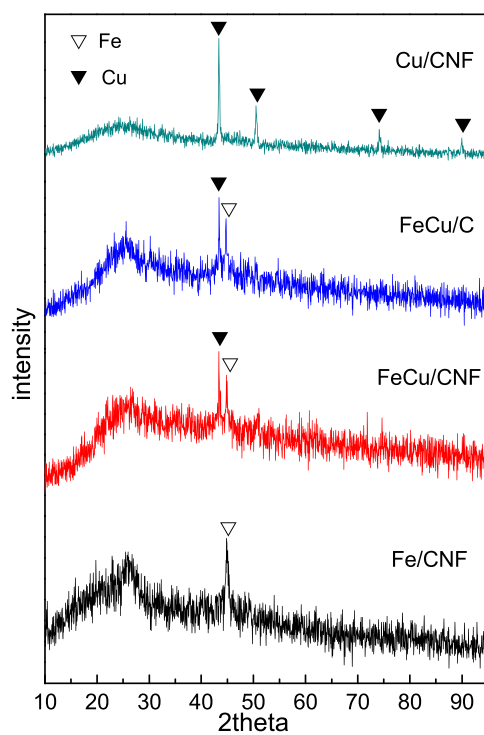


Fig 1. Wide-angle XRD patterns of Fe/CNF, FeCu/CNF, FeCu/C and Cu/CNF.

pared without the electrospinning process. In sharp contrast, the as electron-spun nanofibers (Fe/PANNF, FeCu/PANNF and Cu/PANNF) exhibit straight and continuous fiber structure, with smooth surface and uniform diameter of about 195 nm (Fig. S1A-C and corresponding insets). After stabilization in air at 240 °C for 3 h and carbonization in nitrogen at 900 °C for 2 h, the obtained carbonic samples (Fe/CNF, FeCu/CNF and Cu/CNF) still retain fibrous and regular morphology (Fig. 3A-C). However, these carbon nanofibers seem like a bit more fragile than PAN-based nanofibers, which is similar to the previous reports [47]. Moreover, the average diameter of the obtained carbon nanofibers is about 140 nm (Fig. 3A-C and corresponding insets), which is thinner than untreated fibers. This may be due to the volume shrinkage of PAN and metallic salts decomposition during the thermal treatment [47]. For FeCu/C (Fig. 3D), which derived from FeCu/PAN, displaying the same bulky and ruleless morphology compared with FeCu/PAN.

The interior detailed structure of obtained carbonic samples are further investigated by TEM. As shown in Fig. 4A-C, all fibrous samples (Fe/CNF, FeCu/CNF and Cu/CNF) are uniform and well dispersed at low magnifications. As expected, a piece of bulky carbon is observed in the TEM image of FeCu/C (Fig. 4D). Moreover, from the high magnifications of Fe/CNF, FeCu/CNF, Cu/CNF and FeCu/C (Fig. 4E-H), it can be seen that the dark dots are uniformly dispersed in carbon matrixes, which are corresponding to the metallic nanoparticles, indicating that the metallic nanoparticles can be formed during the carbonization process through the carbothermic reduction. From the corresponding insets in Fig. 4E-H, the average sizes of metallic nanoparticles are 8, 15, 18, and 26 nm for Fe/CNF, FeCu/CNF, Cu/CNF and FeCu/C, respectively. Additionally, the presence of iron-copper bimetallic nanoparticles in FeCu/CNF is further explored by STEM and EDS elemental mapping (Fig. 4I). The corresponding elemental mappings show a very homogeneous distribution, which further confirms the existence of the hybrid iron-copper bimetallic nanoparticles.

Nitrogen adsorption-desorption measurements are performed for evaluating the specific surface area and interior porous structure of the carbonic samples. The corresponding isotherms of nitro-

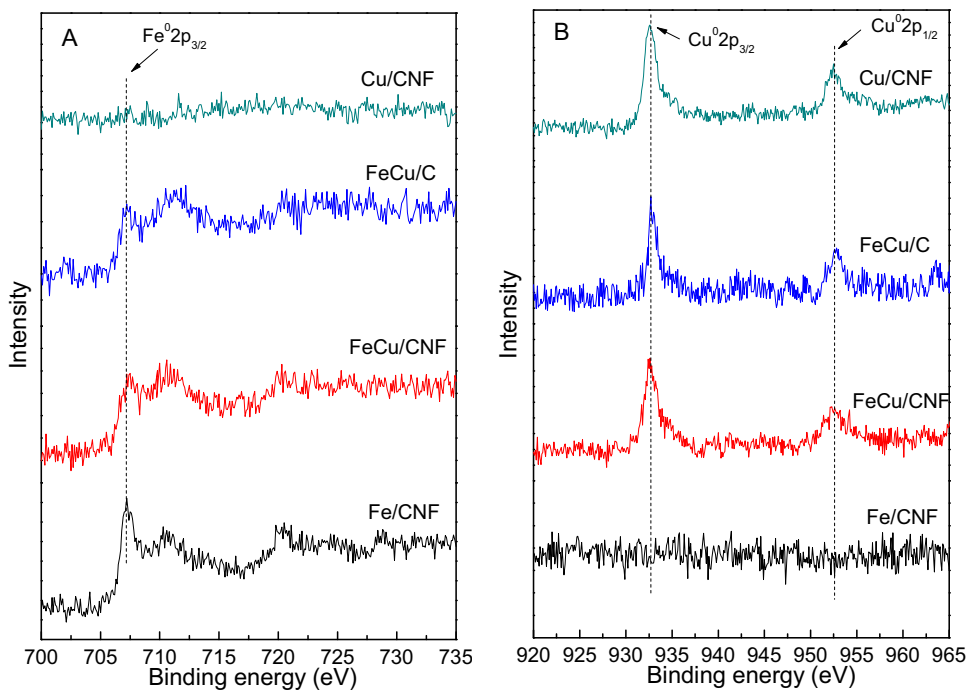


Fig. 2. (A) Fe and (B) Cu XPS of Fe/CNF, FeCu/CNF, FeCu/C and Cu/CNF.

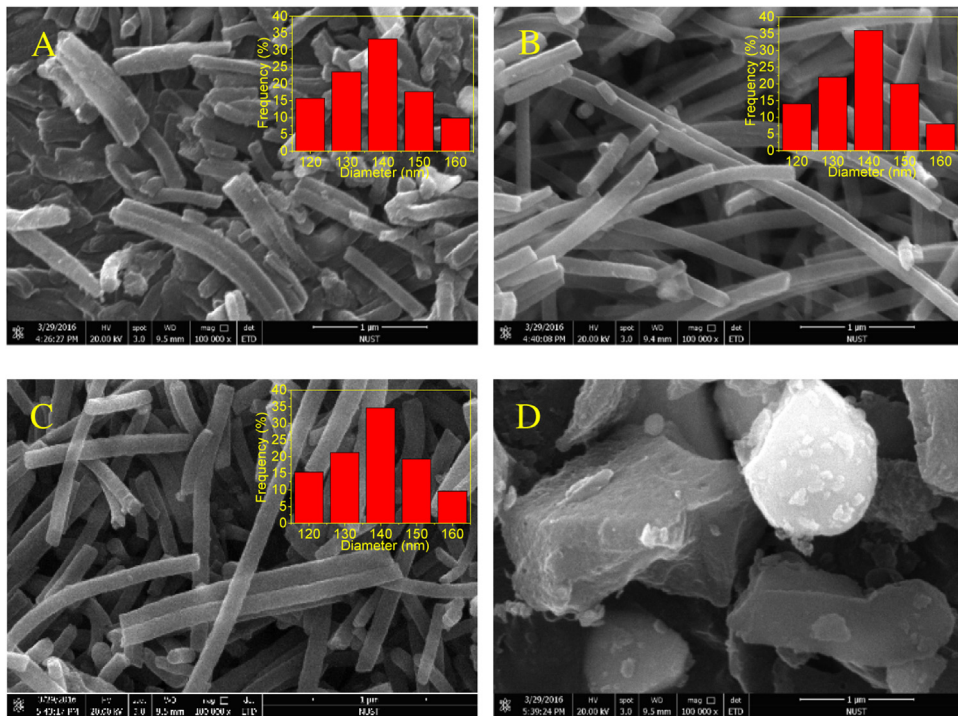


Fig. 3. SEM images of (A) Fe/CNF, (B) FeCu/CNF, (C) Cu/CNF and (D) FeCu/C; the insets in (A), (B) and (C) are distribution histogram of carbon nanofibers diameter calculated from corresponding SEM images.

gen adsorption-desorption and pore size distribution are shown in Fig. 5A and B and Table 1. The BET specific surface area of Fe/CNF, FeCu/CNF, Cu/CNF and FeCu/C are 281, 267, 261 and $266 \text{ m}^2/\text{g}$, respectively. The DFT average pore size of Fe/CNF, FeCu/CNF, Cu/CNF and FeCu/C are 2.4, 1.5, 1.5 and 1.8 nm. And the total pore volume of Fe/CNF, FeCu/CNF, Cu/CNF and FeCu/C are 0.17, 0.15, 0.13 and $0.15 \text{ cm}^3/\text{g}$, respectively. From above results, it can be seen that the specific surface area, average pore size and total pore volume

of all samples are proximate, which imply that the samples possess similar porous structure.

3.2. Catalytic performance on degradation of AOII with different catalysts

The catalytic performance of prepared catalysts were evaluated by degradation of a typical azo dye, AOII. All the experimental con-

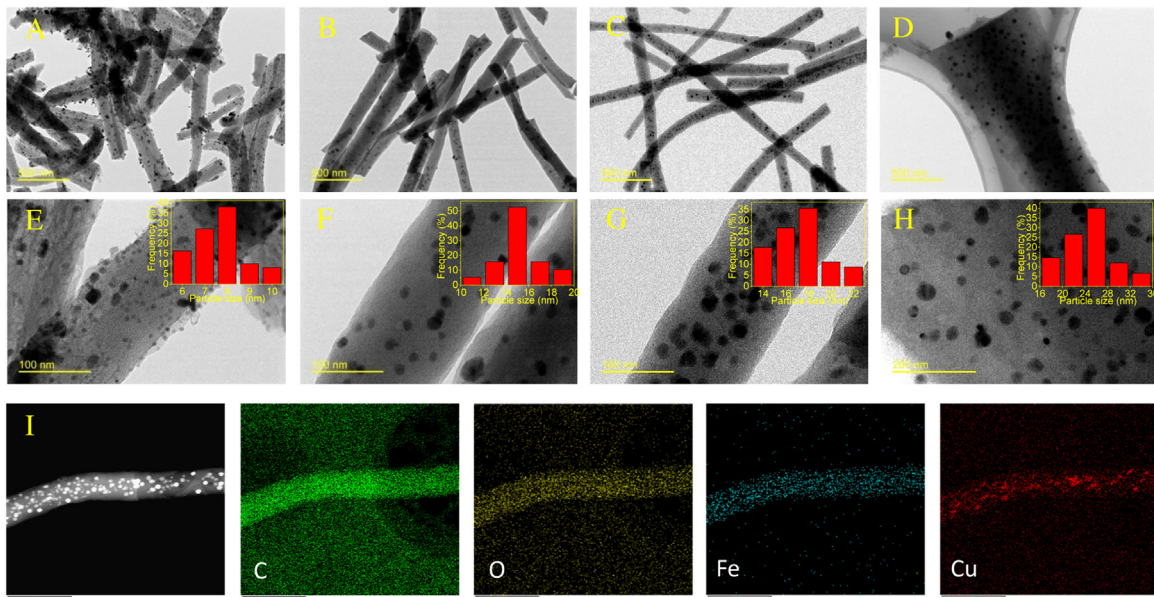


Fig. 4. TEM images of (A and E) Fe/CNF, (B and F) FeCu/CNF, (C and G) Cu/CNF and (D and H) FeCu/C; (I) STEM and elemental mapping images of FeCu/CNF for C, O, Fe and Cu with color superposition; the insets in (E), (F), (G) and (H) are distribution histogram of metallic particle size calculated from corresponding TEM images.

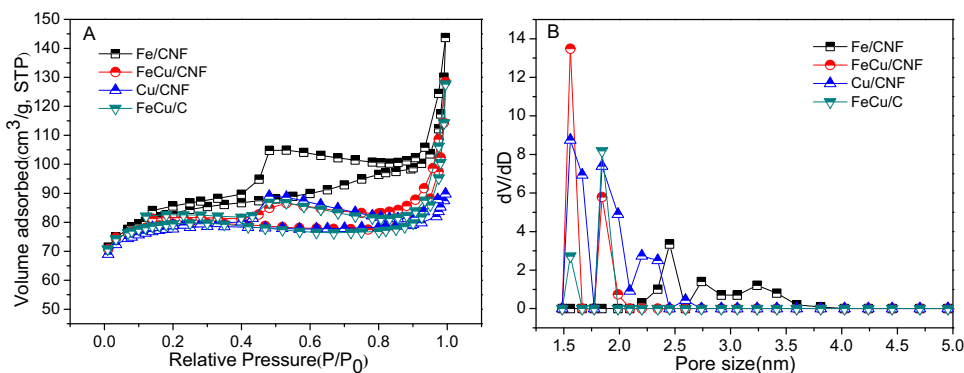


Fig. 5. (A) N_2 adsorption/desorption isotherms and (B) pore size distribution of Fe/CNF, FeCu/CNF, Cu/CNF and FeCu/C.

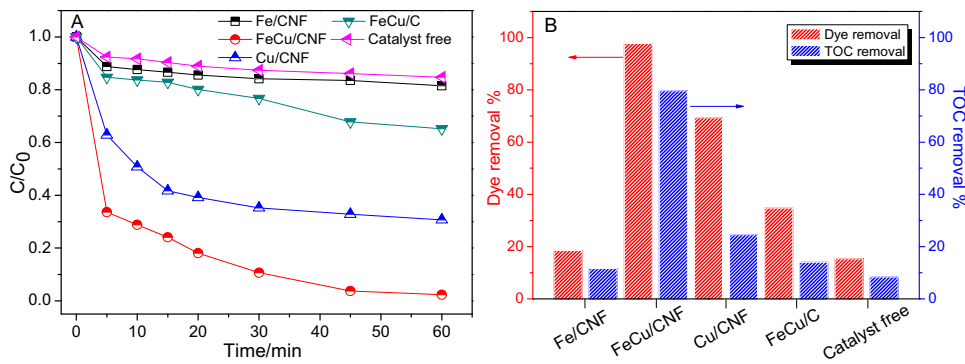


Fig. 6. (A) the removal efficiency of orange II during the reaction and (B) the dye and TOC removal rate at 1 h with different catalysts. The experimental conditions were at pH value of 7.0, 54.8 mM H_2O_2 , 0.5 g/L catalyst dosage, 100 mg/L orange II and temperature 30 °C. (For interpretation of the references to colour in this figure legend, the reader is referred to the web version of this article.)

ditions in this part were conducted at pH of 7, 30 °C, catalyst dosage of 0.5 g/L and 54.8 mM H_2O_2 , with degradation of 100 mg/L AOII. Fig. 6A and B display the process of AOII removal, which obtained by using different catalysts. It can be seen that only 15.3% AOII is removed after 1 h reaction when H_2O_2 alone was present. Meanwhile, the obtained AOII removal by using Fe/CNF and Cu/CNF as

catalysts are 18.5 and 69.3%, respectively, which illustrated that the preferable catalytic activity of Cu/CNF compared with Fe/CNF. Significantly, almost 97.7% of AOII is removed by FeCu/CNF in 1 h, which reflects the prime catalytic activity. This is due to the synergistic effect between iron and copper, which could enhance the catalytic activity of the catalyst in Fenton catalysis [25,28,48]. It

Table 1

Textural properties of synthesized samples.

Sample	S_{BET} (m^2/g) ^a	V_{Total} (cm^3/g) ^b	D_{DFT} (nm) ^c
Fe/CNF	281	0.17	2.4
FeCu/CNF	267	0.15	1.5
Cu/CNF	261	0.13	1.5
FeCu/C	266	0.15	1.8

^a The specific surface areas.^b Total pore volume.^c Pore diameter.

is worthy to note that the heterogeneous Fenton catalytic system from FeCu/CNF also appeared to have a higher degradation efficiency than some previous reported catalysts for removal of AOII, as presented in Table 2 [8,49–51]. Moreover, in order to explore the nanofibrous structure superiority of catalyst in catalytic activity, the FeCu/C catalyst with the same metal component but nonfibrous nanostructure, also has been investigated. Comparing with FeCu/CNF, FeCu/C showed a lower performance in catalytic activity on degradation of AOII. Only 34.8% AOII is removed in FeCu/C catalytic system. This result reveals that the nanofibrous structure has obvious superiority in catalytic activity. It is because that the nanofibrous structures of catalyst could allow a fast and long-distance electron transport and promote the kinetics of electron transfer during the catalytic reaction, which is ascribed to their high axial ratio aspect [34,35]. In addition, to explore the AOII adsorption effect on the heterogeneous Fenton catalytic reaction of various catalysts, the adsorption experiments were set up at pH of 7, 30 °C, catalyst dosage of 0.5 g/L and 100 mg/L AOII. As shown in Fig. S2, the adsorption of AOII are 16.2, 15.4, 15.1 and 15.3% in 1 h reaction time by Fe/CNF, FeCu/CNF, Cu/CNF and FeCu/C, respectively. From the AOII adsorption results, it can be seen that the adsorption ability of catalysts are similar and the difference of AOII removal efficiency is mainly due to the distinction of heterogeneous catalytic activity from various catalysts. Furthermore, to demonstrate the mineralization degree of AOII by the four catalysts and catalyst free system after 1 h reaction, the removal of TOC is shown in Fig. 6B. It can be seen that the removal rate of TOC obtained by Fe/CNF, FeCu/CNF, Cu/CNF, FeCu/C and catalyst free are 11.6, 79.6, 24.5, 14.1 and 8.4%, respectively. Obviously, the AOII is also degraded more completely by using FeCu/CNF, which clearly indicate the excellent catalytic activity of FeCu/CNF.

3.3. Effect of the initial pH of AOII solution

Generally, the iron based catalysts during the Fenton process suffer from relative inert activity when conducted at high pH values. Therefore, it is an urgent need for developing a catalyst, which possesses a wide pH range adapting property. To explore the pH adaptability of FeCu/CNF, the effect of different initial pH values on catalytic activity of catalyst is demonstrated. For comparison, the sample of Fe/CNF also has been investigated. The different initial pH values were set at 2.0, 3.0, 5.0, 7.0, 9.0 and 10.0. The other detailed experimental conditions were set at 30 °C, catalyst dosage 0.5 g/L, H_2O_2 54.8 mM, 100 mg/L AOII. The removal efficiencies of

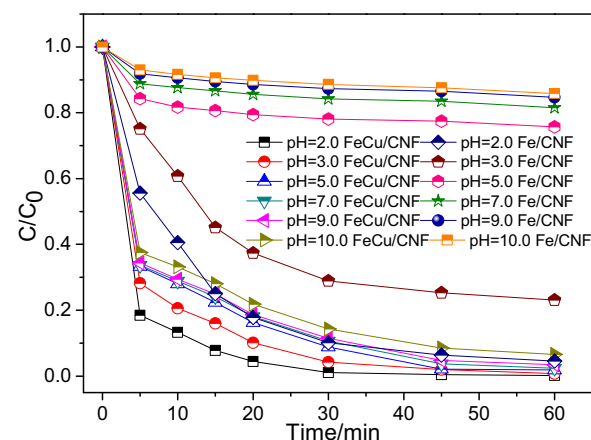


Fig. 7. The removal efficiency of orange II by FeCu/CNF and Fe/CNF with different initial pH values during the reaction in 1 h. The other experimental conditions were fixed on 54.8 mM H_2O_2 , 0.5 g/L catalyst dosage, 100 mg/L orange II and temperature 30 °C. (For interpretation of the references to colour in this figure legend, the reader is referred to the web version of this article.)

AOII are shown in Fig. 7. It can be seen that about 99.8, 99.3, 98.1, 97.7, 96.5 and 93.4% of AOII are removed by FeCu/CNF after 1 h when conducted at pH of 2.0, 3.0, 5.0, 7.0, 9.0 and 10.0, respectively, which reveals proximate catalytic activity at the pH range from 2.0 to 10.0. In contrast, the AOII removal efficiencies are about 95.4, 76.9, 24.3, 18.5, 15.3 and 14.1% by Fe/CNF under the pH of 2.0, 3.0, 5.0, 7.0, 9.0 and 10.0, respectively. Apparently, Fe/CNF shows lower catalytic activity compared with FeCu/CNF, and the catalytic activity of Fe/CNF drops rapidly with the initial pH increased from 2.0 to 10.0. The above results indicate that the catalytic activity of FeCu/CNF is slightly affected by the initial pH of reaction circumstance compared with Fe/CNF, implying a wider pH adaptation ability. It is because that the high standard reduction potential difference (0.78 V) could form the galvanic behavior between Cu (Cu^{2+}/Cu , $E^\theta = 0.34 \text{ V}$) and Fe (Fe^{2+}/Fe , $E^\theta = -0.44 \text{ V}$), which could promote the corrosion rate of Fe in FeCu/CNF system, improve the reactivity of iron and further facilitate the generation of hydroxyl radicals under oxic condition [52–54].

The concentrations of leaching iron and copper ions after 1 h reaction by Fe/CNF and FeCu/CNF during the degradation of orange II in different pH values are shown in Table S1. The results show that the concentrations of leaching iron ions are 0.563, 0.386, 0.128, 0.085, 0.078 and 0.073 mg/L from the Fe/CNF when conducted in 2.0, 3.0, 5.0, 7.0, 9.0 and 10.0 pH values at the end of the reaction, respectively. In the case of FeCu/CNF, the concentrations of leaching iron ions are 0.124, 0.082, 0.031, 0.021, 0.019 and 0.016 mg/L when displayed in 2.0, 3.0, 5.0, 7.0, 9.0 and 10.0 pH values, respectively. And the concentrations of leaching copper ions in FeCu/CNF are 0.436, 0.302, 0.216, 0.211, 0.197 and 0.189 mg/L when conducted in pH values of 2.0, 3.0, 5.0, 7.0, 9.0 and 10.0, respectively. From above results, it can be seen that the concentrations of leaching metal ions are decreased with the increasing of pH values, indicating that the catalysts are more stable in higher pH values. It is worthy to note

Table 2

AOII degradation over different heterogeneous Fenton catalysts.

Catalyst	Extra power supply	C_{AOII} (mg/L) ^a	D_{Catalyst} (g/L) ^b	Removal (%)	Time (min)	Refs.
Fe ₂ O ₃ /HPS	Visible light	35	0.5	91.5	180	[49]
ZnFe ₂ O ₄	Visible light	100	0.5	94.9	60	[50]
Fe-Co/SAB-15	Ultrasound	105	1.0	95.5	120	[51]
2Fe6Cu/HMS	–	100	1.0	92.8	120	[8]
FeCu/CNF	–	100	0.5	97.7	60	This work

^a The concentration of AOII.^b The dosage of catalyst.

that all the concentrations of leaching metal ions are lower than the legal limit imposed by the European Union (2 mg/L) [19].

To investigate the contribution of leaching iron and copper ions on the degradation of AOII in Fe/CNF and FeCu/CNF Fenton catalytic systems, the experiments in homogeneous systems at different pH values were carried out. The catalysts were firstly added in corresponding pH values of AOII solutions. After vigorous agitation for 1 h, the Fe/CNF and FeCu/CNF catalysts were removed and then adding 56 μ L H₂O₂ (30%) into the filtrate. Thus, the homogeneous systems were established to further reaction 1 h. As shown in Fig. S3, for Fe/CNF, the removal of AOII are 22.4, 20.4, 17.8, 17.1, 14.7 and 14.0% when conducted in the pH values of 2.0, 3.0, 5.0, 7.0, 9.0 and 10.0, respectively. And the corresponding removal of AOII by adsorption in Fe/CNF system are 16.7, 16.5, 16.4, 16.2, 13.9, 13.3% when displayed in the pH values of 2.0, 3.0, 5.0, 7.0, 9.0 and 10.0, respectively. Therefore, the corresponding contribution of homogeneous Fenton catalysis in Fe/CNF system are 5.7, 3.9, 1.4, 0.9, 0.8 and 0.7% when conducted in the pH values of 2.0, 3.0, 5.0, 7.0, 9.0 and 10.0, respectively. In the case of FeCu/CNF, the removal efficiencies of AOII are 20.7, 19.1, 18.0, 17.7, 15.3 and 15.1% when displayed in the pH values of 2.0, 3.0, 5.0, 7.0, 9.0 and 10.0, respectively. And the corresponding removal of AOII by adsorption in FeCu/CNF system are 15.8, 15.7, 15.6, 15.4, 13.1 and 13.0% when conducted in the pH values of 2.0, 3.0, 5.0, 7.0, 9.0 and 10.0, respectively. Therefore, the corresponding contribution of homogeneous Fenton catalysis in FeCu/CNF system are 4.9, 3.4, 2.4, 2.3, 2.2, 2.1% when displayed in the pH values of 2.0, 3.0, 5.0, 7.0, 9.0 and 10.0, respectively. Based on the heterogeneous and homogeneous Fenton catalytic reaction results, it can be seen that the contribution of homogeneous Fenton catalytic reaction is a little in both Fe/CNF and FeCu/CNF Fenton systems. Moreover, the contribution of AOII removal in Fe/CNF Fenton system is mainly by adsorption when the pH values are above 5. In contrast, the removal of AOII in FeCu/CNF Fenton system is mainly dominated by heterogeneous reaction in various pH values.

3.4. Effect of parameters on catalytic activity of FeCu/CNF for degradation of AOII

3.4.1. Effect of H₂O₂ dosage

The effect of H₂O₂ dosage on catalytic activity of FeCu/CNF for AOII removal is examined in five different H₂O₂ concentrations (13.7, 27.4, 54.8, 109.6 and 219.2 mM, respectively). From Fig. 8A, the AOII removal efficiency is decayed by the increasing H₂O₂ dosage in first 15 min. This may be due to the fact that at the initial reaction stage, the relative low concentration of H₂O₂ could facilitate a much more effective utilization of H₂O₂ [55]. However, after reaction for 1 h, the AOII removal rate is enhanced from 93.3 to 97.7% by increasing H₂O₂ dosage from 13.7 to 54.8 mM, and the AOII removal rate is decreased from 97.7 to 94.0% with the H₂O₂ dosage further increased from 54.8 to 219.2 mM, which is achieved the optimal dosage of H₂O₂ at 54.8 mM. It may be ascribed to the fact that more •OH would be generated when the increased H₂O₂ is in the appropriate range [24], nevertheless, excessive H₂O₂ would be unprofitably consumed due to its scavenging effect (Eqs. (1) and (2)) [25].



3.4.2. Effect of catalyst dosage

The effect of catalyst dosage on catalytic activity of FeCu/CNF for AOII removal is also investigated. The experiments were conducted at five different catalyst dosages, 0.25, 0.5, 1, 1.5 and 2 g/L, respectively. As shown in Fig. 8B, it can be seen that the AOII removal efficiency is enhanced with the increasing of catalyst dosage during

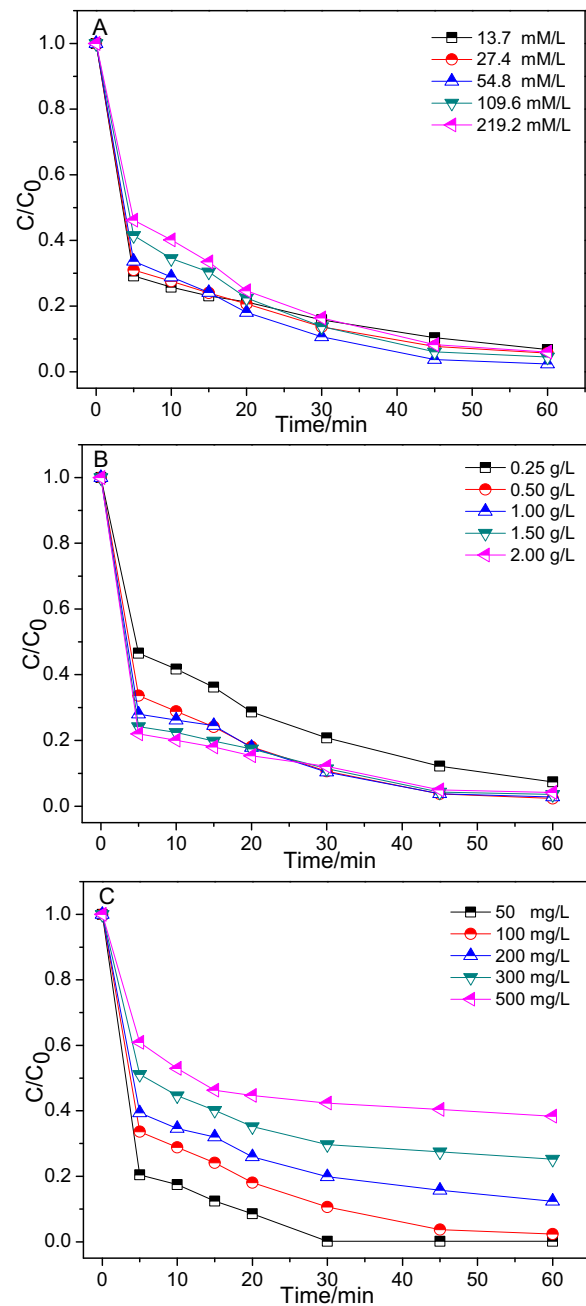


Fig. 8. Effect of parameters on catalytic activity of FeCu/CNF for degradation of orange II during the reaction in 1 h: (A) effect of H₂O₂ dosage, (B) effect of catalyst dosage, (C) effect of initial dye concentration. Except for the investigated parameters, other parameters were fixed on pH value of 7.0, 54.8 mM H₂O₂, 0.5 g/L catalyst dosage, 100 mg/L orange II and temperature 30 °C. (For interpretation of the references to colour in this figure legend, the reader is referred to the web version of this article.)

the first 20 min. It may be attributed to the fact that more amount of catalyst provides more active sites to adsorb and catalyze H₂O₂ at the initial stage of reaction and thus generate higher amount of •OH [55]. However, after reaction for 1 h, the AOII removal rate is attained to 92.6% under the condition with catalyst dosage of 0.25 g/L, and the AOII removal rate is decreased from 97.7 to 95.8% with the H₂O₂ dosage increase from 0.5 to 2.0 g/L. From the above results, it can be seen that the excessive dosage of catalyst has an adverse effect on AOII removal efficiency, which may ascribe to the fact that unit surface adsorption of H₂O₂ and the density of surface

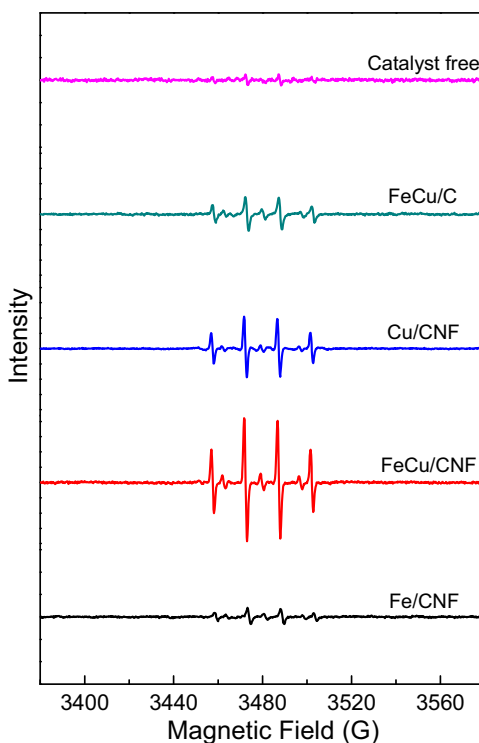


Fig. 9. DMPO spin trapping ESR spectra of hydroxyl radicals generated by different catalysts.

adsorbed H_2O_2 on catalyst surface would be decreased [56]. Thus, the optimal dosage in degradation of AOII by FeCu/CNF is 0.5 g/L.

3.4.3. Effect of initial dye concentration

The effect of the initial dye concentration on the catalytic activity of FeCu/CNF for AOII removal is shown in Fig. 8C. Five initial dye concentration were executed. The dye removal rate are 99.8, 97.7, 87.6, 74.8 and 61.7% when conducted at initial dye concentration of 50, 100, 200, 300 and 500 mg/L, respectively, after reaction for 1 h. It can be observed that the AOII removal efficiency is decreased with the increasing of initial dye concentration, and is more limited in a higher initial AOII concentration. This is because in higher concentration of dye, there is more intense competitive adsorption among dye molecules due to the limited reaction area of catalyst [55]. In addition, the more intermediates could be produced in the case of higher dye concentration, which would reduce the effective utilization of active surface sites for H_2O_2 and dye molecules [52]. Despite of this, the total amount of removed AOII is enhanced with the initial dye concentration increased. Specifically, 49.9, 97.7, 175.2, 224.4 and 308.5 mg of AOII are removed when initial concentration of dye are 50, 100, 200, 300 and 500 mg/L, respectively.

3.5. Possible mechanisms

To ascertain the active radicals in the catalytic reactions, Electron spin resonance (ESR) spectroscopy was performed by using 5,5-dimethyl-1-pyrroline N-oxide (DMPO) as trapping agent. As shown in Fig. 9, all the ESR spectrograms exhibit a 4-fold characteristic peaks with an intensity ratio of 1:2:2:1 and with $a^N = a^H = 14.9 \text{ G}$, which corresponding to the typical signal of DMPO-•OH adduct compared with standard DMPO-•OH peaks in previous reports [36–38]. These results indicate that all catalysts could catalyze H_2O_2 to generate •OH and the •OH is main active radical in these heterogeneous Fenton reactions. Moreover, it is worthy to note that the intensity of DMPO-•OH peaks by using FeCu/CNF as

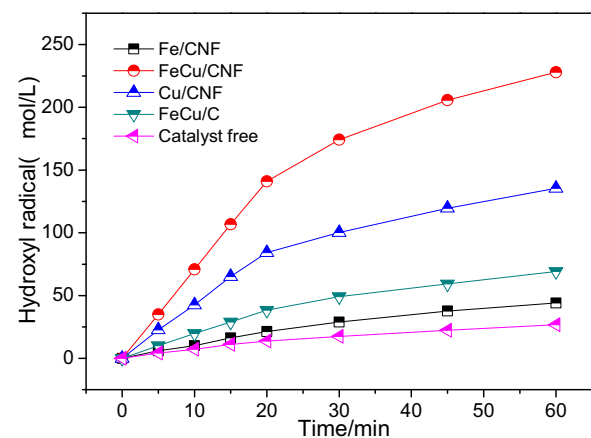
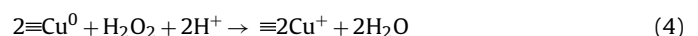
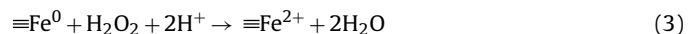


Fig. 10. Generation of hydroxyl radicals with different catalysts during the reaction in 1 h. The experimental conditions were at pH value of 7.0, 54.8 mM H_2O_2 , 0.5 g/L catalyst dosage and temperature 30 °C.

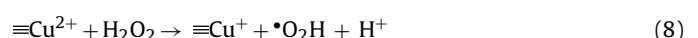
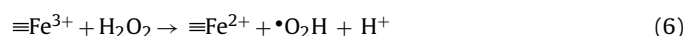
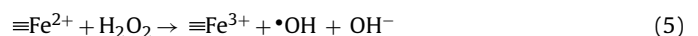
catalyst is much higher than Fe/CNF, Cu/CNF, FeCu/C and catalyst free, illustrating that more higher catalytic activity possessed by FeCu/CNF.

In order to quantify the cumulative amount of •OH, benzoic acid, which can react with •OH with a reaction rate constant of $4.2 \times 10^9 \text{ M}^{-1}\text{s}^{-1}$ [57], was used as a probe molecule. The p-HBA can be obtained in above reaction and per mole p-HBA can be generated quantitatively by $5.87 \pm 0.18 \text{ mol } \cdot\text{OH}$ [58]. The p-HBA can be quantitative determined by HPLC and the amount of •OH can be calculated from the amount of p-HBA. The cumulative amount of •OH generated by various catalysts are presented in Fig. 10, it can be observed that the cumulative amount of •OH produced by Fe/CNF, FeCu/CNF, Cu/CNF, FeCu/C and catalyst free are 44.1, 228.0, 135.5, 69.2 and $26.7 \mu\text{mol L}^{-1}$ after reaction for 1 h, respectively. Obviously, the cumulative amount of •OH produced by FeCu/CNF is up to the highest value, which is almost 5.2, 1.7, 3.3 and 8.5 times than Fe/CNF, Cu/CNF, FeCu/C and catalyst free, respectively. Therefore, FeCu/CNF possesses the best ability of producing •OH, which is consistent with the tendency of AOII removal efficiency and the intensity tendency of DMPO-•OH peaks.

Previous investigations have shown that the •OH is the major active radical and plays important role in the heterogeneous Fenton reaction [59,60]. The above results illustrate that the enhanced catalytic activity is displayed by catalyst of FeCu/CNF, which shows excellent ability of producing •OH and high AOII removal efficiency. Based on all above experimental results, a possible mechanism for FeCu/CNF degradation of AOII has been proposed. In the first step, the H_2O_2 molecules can be adsorbed on FeCu/CNF and reacted with the metallic nanoparticles. Specifically, the Fe^0 can be oxidized to Fe^{2+} via a two electron transfer (Eq. (3)) and Cu^0 oxidized to Cu^+ via a one electron transfer from the nanoparticles surface to H_2O_2 (Eq. (4)) [15,25].



Then, H_2O_2 can be active by Fe^{2+} to produce •OH according to the Haber-Weiss mechanism [59,60]. Similarly, H_2O_2 can also be activated by Cu^+ to generate •OH [25,61]. The reaction equations are displayed as follows: (Eqs. (5)–(8))



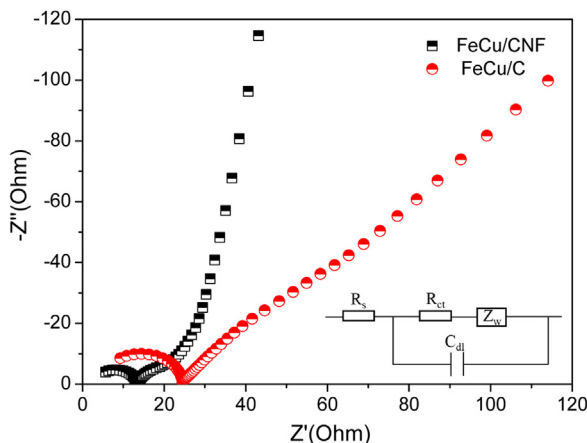
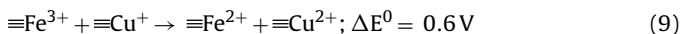


Fig. 11. Electrochemical impedance spectroscopy (EIS) spectra of FeCu/CNF and FeCu/C.



Meanwhile, the produced Fe^{3+} can also be reduced to Fe^{2+} by Cu^+ attributed to the potential difference (0.6 V) between $\text{Fe}^{3+}/\text{Fe}^{2+}$ (0.77 V) and $\text{Cu}^{2+}/\text{Cu}^+$ (0.17 V) (Eq. (9)) [19,25]. The synergistic effect arises from a combination of enhanced peroxide decomposition and faster redox processes driven through the reduction of Fe^{3+} by Cu^+ [28]. Therefore, the electrochemically accessible sites, interfacial electron transfer and redox reaction kinetics are greatly enhanced in FeCu/CNF by redox cycles of $\text{Fe}^{3+}/\text{Fe}^{2+}$ and $\text{Cu}^{2+}/\text{Cu}^+$ pair [8], and thus more $\cdot\text{OH}$ would be generated to attack more AOII molecules compared with monometallic catalysts such as Fe/CNF or Cu/CNF.

Furthermore, the nanofibrous structure of catalyst also plays a vital role in catalytic activity of FeCu/CNF during the heterogeneous Fenton reaction. On the basis of above results, the FeCu/CNF shows higher catalytic activity than FeCu/C. Interestingly, the main difference between two catalysts is the morphology of support. Specifically, the FeCu/CNF is based on the nanofibrous structure, whereas, FeCu/C is bulky and ruleless. According to the previous reports [34,35], nanofibrous structures of catalyst could show a superior catalytic activity because of their high axial ratio aspect, which allow a fast and long-distance electron transport and promote the kinetics of electron transfer during the catalytic reaction. To prove the transport ability of electron, EIS measurements were carried out. The Nyquist plots of FeCu/CNF and FeCu/C are shown in Fig. 11. A typical quasi-semicircle and a linear portion can be observed in EIS spectra, which is ascribed to the charge-transfer resistance in high frequency region and mass transfer process resistance in low frequency region, respectively [62]. Obviously, the diameter of semicircle in FeCu/CNF is much smaller than that of FeCu/C, indicating that the charge-transfer resistance of FeCu/CNF is significantly decreased compared to the bulk FeCu/C, further suggesting the enhanced performance of the electron transfer in FeCu/CNF [63]. In addition, the slope of the FeCu/CNF is much closer to y axis at low frequency region, this reveals that electron transfer encounters less diffusion resistance compared with FeCu/C, which could promote the electron transfer rate [63,64]. Moreover, based on the semicircles obtained by FeCu/CNF and FeCu/C, the charge transfer resistance (R_{ct}) in parallel with double-layer capacitance (C_{dl}) can be fitted and interpreted by an equivalent electric circuit. The fitted value of R_{ct} in FeCu/CNF is 9.52Ω , which is much lower than 20.44Ω obtained by FeCu/C. Therefore, the nanofibrous structure makes a great contribution to the excellent catalytic activity of catalyst. The superiority of nanofibrous structure in FeCu/CNF on catalytic activity is due to the large enhancement in overall

conductivity, which can accelerate electron transfer and ultimately improve the catalytic activity of the catalyst. Based on the results of $\cdot\text{OH}$ detection and resistance of mass transfer testing in catalysts, the remarkable catalytic performance of FeCu/CNF is considered as the synergistic effect of iron and copper and the superiority of nanofibrous structure in catalyst.

3.6. The stability and recyclability of catalyst

In order to investigate the long term stability of the catalyst, FeCu/CNF was used in five consecutive runs. As shown in Fig. 12, the removal rates of AOII after 1 h at each turn are 97.7, 92.5, 87.0, 82.7 and 79.9%, respectively. Compared with the first run in removing of AOII, the removal rate of AOII has been decreased by 17.8% in fifth run. As previous reports [65,66], the slightly decreased catalytic activity of catalyst is a normal phenomenon in consecutive experiments performed in catalytic reaction, which may be ascribed to the active constituent leaching from catalyst and catalyst poisoning caused by intermediates. To gain an insight into the reason of decreased catalytic activity from FeCu/CNF, the SEM and TEM images of FeCu/CNF after five consecutive runs are shown in Fig. S4. From Fig. S4, it can be seen that the morphology and the interior structure of used FeCu/CNF are similar with the fresh FeCu/CNF and there is no obvious change with the metallic nanoparticles. This result is consistent with the results that low leaching metal ions are observed during the Fenton catalytic reaction (Table S1). Therefore, the decreased catalytic activity of FeCu/CNF after consecutive runs is considered as the catalyst poisoning, which may be caused by the intermediates produced during the catalytic reaction. Significantly, the fifth run of AOII removal efficiency still remains 79.9%. The above results demonstrate that the fabricated catalyst exhibits a good recyclability performance.

4. Conclusions

In the present work, an iron-copper bimetal-based carbon nanofibers composite catalyst was prepared by electrospinning technique and followed by the carbonization of electrospun nanofibers. The iron-copper bimetallic nanoparticles were formed in situ by carbothermic reduction during the carbonization process. The catalyst possesses a fibrous morphology, porous structure with high specific surface area, and the iron-copper nanoparticles are highly dispersed in the matrix of carbon nanofibers, which can be illustrated by XRD, XPS, nitrogen physisorption, SEM and TEM. The enhanced catalytic activity of catalyst for AOII removal is observed, it is found that the addition of copper could improve the catalytic activity, make the catalyst less pH dependent. The nanofibrous structure of catalyst also make a positive contribution in catalytic activity. The stability and recoverability of FeCu/CNF were also investigated, which exhibited a good performance even after 5 consecutive runs. The as-synthesized catalyst is proved to be an attractive candidate in heterogeneous Fenton chemistry and can provide a new strategy in development of novel effective Fenton catalysts.

Acknowledgements

This work was financially supported by the National Natural Science Foundation of China (Grant no. 5147224) and the priority academic program development of Jiangsu higher education institutions.

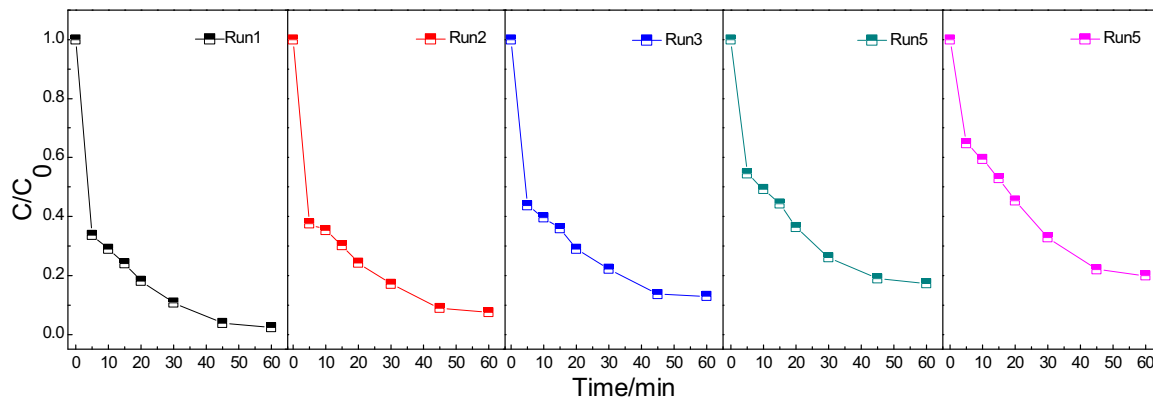


Fig. 12. Degradation of orange II in different batch runs in the FeCu/CNF system. (For interpretation of the references to colour in this figure legend, the reader is referred to the web version of this article.)

Appendix A. Supplementary data

Supplementary data associated with this article can be found, in the online version, at <http://dx.doi.org/10.1016/j.apcatb.2017.02.032>.

References

- [1] A.D. Levine, T. Asano, Environ. Sci. Technol. 38 (2004) 201A.
- [2] X.N. Li, J.Y. Liu, A.I. Rykov, H.X. Han, C.Z. Jin, X. Liu, J.H. Wang, Appl. Catal. B: Environ. 179 (2015) 196–205.
- [3] X. Li, F.Y. Gai, B.Y. Guan, Y. Zhang, Y.L. Liu, Q.S. Huo, J. Mater. Chem. A 3 (2015) 3988–3994.
- [4] M. Arslan, S. Sayin, M. Yilmaz, Water Air Soil Pollut. 224 (2013) 1–9.
- [5] Y.F. Su, Z. Wu, Y.N. Wu, J.D. Yu, L. Sun, C.J. Lin, J. Mater. Chem. A 3 (2015) 8537–8544.
- [6] W. Jo, S. Kumar, M.A. Isaacs, A.F. Lee, S. Karthikeyan, Appl. Catal. B: Environ. 201 (2017) 159–168.
- [7] Y.W. Gao, Y. Wang, H. Zhang, Appl. Catal. B: Environ. 178 (2015) 29–36.
- [8] J. Wang, C. Liu, I. Hussain, C. Li, J.S. Li, X.Y. Sun, J.Y. Shen, W.Q. Han, L.J. Wang, RSC Adv. 6 (2016) 54623–54635.
- [9] P.P. Qiu, W. Li, B. Thokchom, B. Park, M.C. Cui, D.Y. Zhao, J. Khim, J. Mater. Chem. A 3 (2015) 6492–6500.
- [10] J.L. Wang, L.J. Xu, Crit. Rev. Environ. Sci. Technol. 42 (2011) 251–325.
- [11] K. Rusevova, F.D. Kopinke, A. Georgi, J. Hazard. Mater. 241–242 (2012) 433–440.
- [12] H.Y. Min, X.Q. Ran, J.W. Fan, Y. Sun, J.P. Yang, W. Teng, W.X. Zhang, G.M. Li, D.Y. Zhao, J. Mater. Chem. A 3 (2015) 7399–7405.
- [13] Y.H. Zhan, X.A. Zhou, B. Fu, Y.L. Chen, J. Hazard. Mater. 187 (2011) 348–354.
- [14] J. Wang, C. Liu, L. Tong, J.S. Li, R. Luo, J.W. Qi, Y. Li, L.J. Wang, RSC Adv. 5 (2015) 69593–69605.
- [15] A. Dhakshinamoorthy, S. Navalon, M. Alvaro, H. Garcia, ChemSusChem 5 (2012) 46–64.
- [16] J.G. Shi, Z.H. Ai, L.Z. Zhang, Water Res. 59 (2014) 145–153.
- [17] M. Munoz, Z.M. de Pedro, J.A. Casas, J.J. Rodriguez, Appl. Catal. B: Environ. 176 (2015) 249–265.
- [18] L.G. Devi, K.S.A. Raju, S.G. Kumar, K.E. Rajashekhar, J. Taiwan Inst. Chem. Eng. 42 (2011) 341–349.
- [19] Y.B. Wang, H.Y. Zhao, M.F. Li, J.Q. Fan, G.H. Zhao, Appl. Catal. B: Environ. 147 (2014) 534–545.
- [20] Y.X. Wang, H.Q. Sun, X.G. Duan, H.M. Ang, M.O. Tadé, S.B. Wang, Appl. Catal. B: Environ. 172 (2015) 73–81.
- [21] J.Y. Cai, H. Ma, J.J. Zhang, Q. Song, Z.T. Du, Y.Z. Huang, J. Xu, Chem. Eur. J. 19 (2013) 14215–14223.
- [22] B.B. Fan, H.Y. Li, W.B. Fan, C. Jin, R.F. Li, Appl. Catal. A: Gen. 340 (2008) 67–75.
- [23] M.N. Timofeeva, S.T. Khankhasaeva, E.P. Talsi, V.N. Panchenko, A.V. Golovin, E.T. Dashinamzhilova, S.V. Tsybulya, Appl. Catal. B: Environ. 90 (2009) 618–627.
- [24] M. Xia, M.C. Long, Y.D. Yang, C. Chen, W.M. Cai, B.X. Zhou, Appl. Catal. B: Environ. 110 (2011) 118–125.
- [25] Y.B. Wang, H.Y. Zhao, G.H. Zhao, Appl. Catal. B: Environ. 164 (2015) 396–406.
- [26] S. Karthikeyan, A. Titus, A. Gnanamani, A.B. Mandal, G. Sekaran, Desalination 281 (2011) 438–445.
- [27] S. Karthikeyan, R. Boopathy, G. Sekaran, J. Colloid Interf. Sci. 448 (2015) 163–174.
- [28] S. Karthikeyan, M.P. Pachamuthu, M.A. Isaacs, S. Kumar, A.F. Lee, G. Sekaran, Appl. Catal. B: Environ. 199 (2016) 323–330.
- [29] L. Luo, C. Dai, A. Zhang, J. Wang, M. Liu, C. Song, X. Guo, Catal. Sci. Technol. 5 (2015) 3159–3165.
- [30] C.M.A. Parlett, K. Wilson, A.F. Lee, Chem. Soc. Rev. 42 (2013) 3876–3893.
- [31] A. Yousef, N.A.M. Barakat, M.E. Newehy, H.Y. Kim, Int. J. Hydrogen Energy 37 (2012) 17715–17723.
- [32] Y.P. Huang, Y.E. Miao, S.S. Ji, W.W. Tjiu, T.X. Liu, ACS Appl. Mater. Interfaces 6 (2014) 12449–12456.
- [33] A. Greiner, J.H. Wendorff, Angew. Chem. Int. Ed. 46 (2007) 5670–5703.
- [34] X.Q. Zhang, Q. Sun, W. Dong, D. Li, A.H. Lu, J.Q. Mu, W.C. Li, J. Mater. Chem. A 1 (2013) 9449–9455.
- [35] L. Wu, X. Zhang, H. Ju, Anal. Chem. 79 (2006) 453–458.
- [36] S. Karthikeyan, D.D. Dionysiou, A.F. Lee, S. Suvitha, P. Maharaja, K. Wilson, G. Sekaran, Catal. Sci. Technol. 6 (2016) 530–544.
- [37] M.P. Pachamuthu, S. Karthikeyan, R. Maheswari, A.F. Lee, A. Ramanathan, Appl. Surf. Sci. 393 (2017) 67–73.
- [38] S. Karthikeyan, G. Sekaran, Phys. Chem. Chem. Phys. 16 (2014) 3924–3933.
- [39] D. Liu, Q.H. Guo, H.Q. Hou, O. Niwa, T.Y. You, ACS Catal. 4 (2014) 1825–1829.
- [40] J.S. Xie, Q.S. Wu, D.F. Zhao, Carbon 50 (2012) 800–807.
- [41] M.E. Lindsey, M.A. Tarr, Chemosphere 41 (2000) 409–417.
- [42] X. Sun, Y.B. Yan, J.S. Li, W.Q. Han, L.J. Wang, J. Hazard. Mater. 266 (2014) 26–33.
- [43] J.S. Li, S.L. Li, Y.J. Tang, M. Han, Z.H. Dai, J.C. Bao, Y.Q. Lan, Chem. Commun. 51 (2015) 2710–2713.
- [44] X. Zhang, S. Lin, Z.L. Chen, M. Megharaj, R. Naidu, Water Res. 45 (2011) 3481–3488.
- [45] S.R. Kanel, B. Manning, L. Charlet, H. Choi, Environ. Sci. Technol. 39 (2005) 1291–1298.
- [46] H. Li, C.Y. Guo, C.L. Xu, Biosens. Bioelectron. 63 (2015) 339–346.
- [47] L. Wang, Y. Yu, P.C. Chen, D.W. Zhang, C.H. Chen, J. Power Sources 183 (2008) 717–723.
- [48] F.L.Y. Lam, X.J. Hu, Catal. Commun. 8 (2007) 2125–2129.
- [49] Z.H. Miao, S.Y. Tao, Y.C. Wang, Y.X. Yu, C.G. Meng, Y.L. An, Micropor. Mater. 176 (2013) 178–185.
- [50] C. Cai, Z.Y. Zhang, J. Liu, N. Shan, H. Zhang, D.D. Dionysiou, Appl. Catal. B: Environ. 182 (2016) 456–468.
- [51] C. Cai, H. Zhang, X. Zhong, L.W. Hou, J. Hazard. Mater. 283 (2015) 70–79.
- [52] Y. Yuan, H.Q. Li, B. Lai, P. Yang, M. Gou, Y.X. Zhou, G.Z. Sun, Ind. Eng. Chem. Res. 53 (2014) 2605–2613.
- [53] L.F. Greenlee, J.D. Torrey, R.L. Amaro, J.M. Shaw, Environ. Sci. Technol. 46 (2012) 12913–12920.
- [54] K.S. Wang, C.L. Lin, M.C. Wei, H.H. Liang, H.C. Li, C.H. Chang, Y.T. Fang, S.H. Chang, J. Hazard. Mater. 182 (2010) 886–895.
- [55] C. Cai, H. Zhang, X. Zhong, L.W. Hou, Water Res. 66 (2014) 473–485.
- [56] R.X. Huang, Z.Q. Fang, X.M. Yan, W. Cheng, Chem. Eng. J. 197 (2012) 242–249.
- [57] G.V. Buxton, C.L. Greenstock, W.P. Helman, A.B. Ross, J. Phys. Chem. 17 (1988) 513–886 (Ref. Data).
- [58] Y.J. Wang, H.Y. Zhao, J.X. Gao, G.H. Zhao, Y.G. Zhang, Y.L. Zhang, J. Phys. Chem. C 116 (2012) 7457–7463.
- [59] S.S. Lin, M.D. Gurol, Environ. Sci. Technol. 32 (1998) 1417–1423.
- [60] W.P. Kwan, B.M. Voelker, Environ. Sci. Technol. 37 (2003) 1150–1158.
- [61] L.L. Zhang, Y.L. Nie, C. Hu, J.H. Qu, Appl. Catal. B: Environ. 125 (2012) 418–424.
- [62] M.Y. Wang, J.R. Huang, M. Wang, D.G. Zhang, W.M. Zhang, W.H. Li, J. Chen, Electrochem. Commun. 34 (2013) 299–303.
- [63] C.X. Wang, P.H. Shi, X.D. Cai, Q.J. Xu, X.J. Zhou, X.L. Zhou, D. Yang, J.C. Fan, Y.L. Min, H.H. Ge, W.F. Yao, J. Phys. Chem. C 120 (2016) 336–344.
- [64] C. Liu, J. Wang, J.S. Li, R. Luo, J.Y. Shen, X.Y. Sun, W.Q. Han, L.J. Wang, ACS Appl. Mater. Interfaces 7 (2015) 18609–18617.
- [65] J.A. Zazo, J.A. Casas, A.F. Mohedano, J.J. Rodríguez, Appl. Catal. B: Environ. 65 (2006) 261–268.
- [66] S. Navalon, M. Alvaro, H. Garcia, Appl. Catal. B: Environ. 99 (2010) 1–26.